Prompt and delayed spectroscopy of ^{142}Tb using recoil-isomer tagging

P. J. R. Mason,[1] D. M. Cullen,[1] C. Scholey,[2] S. Eeckhaudt,[2] T. Grahn,[2,*] P. T. Greenlees,[2] U. Jakobsson,[2]
P. M. Jones,[2] R. Julin,[2] S. Juutinen,[2] S. Ketelhut,[2] A. M. Kishada,[1] M. Leino,[2] A.-P. Leppänen,[2,†]
K. Mäntyniemi,[2] P. Nieminen,[2] M. Nyman,[2] J. Pakarinen,[2,*] P. Peura,[2] P. Rahkila,[2] S. V. Rigby,[1,*]
J. Sarén,[2] J. Sorri,[2] J. Uusitalo,[2] B. J. Varley,[1] and M. Venhart[2,3,‡]

[1]*Schuster Laboratory, University of Manchester, Manchester M13 9PL, United Kingdom*
[2]*Department of Physics, University of Jyväskylä, FIN-40014 Jyväskylä, Finland*
[3]*Department of Nuclear Physics and Biophysics, Comenius University, 84248 Bratislava, Slovakia*
(Received 24 November 2008; published 25 February 2009)

Recoil-isomer tagging has been used to characterize the states built upon an $I^\pi = 8^+$ isomer in ^{142}Tb. High-spin states of the neutron-deficient nucleus ^{142}Tb were populated using an ^{54}Fe beam, accelerated onto a ^{92}Mo target of thickness $\sim$500 μg/cm^2 at energies of 245, 252, and 265 MeV using the K130 cyclotron at the University of Jyväskylä, Finland. Use of the JUROGAM target-position Ge-detector array coupled with the GREAT focal-plane spectrometer at the RITU gas-filled recoil separator has significantly increased the efficiency of the isomer-tagging technique. The rotational band built upon the $I^\pi = 8^+$ isomeric state was established with isomer-tagged γ-γ coincidence data and angular distributions were measured for some of the more intensely populated states. Two previously unobserved bands that bypass the isomer were also established. The new data have been interpreted within the framework of the cranked-shell model. The data show good agreement with the calculated triaxial nuclear shape with $\gamma = -30^\circ$ for the ^{142m2}Tb isomeric state. The $B(M1)/B(E2)$ branching ratios, nuclear alignment, signature splitting, and reduced transition probability, $B(E1)$, of the isomeric state have been systematically compared with those of the neighboring nuclei. These comparisons give further evidence for the $\pi h_{11/2} \otimes \nu h_{11/2}$ configuration of the isomer.

I. INTRODUCTION

Mass $A \approx 140$ nuclei on the neutron-deficient side of stability are known to show softness with respect to the γ deformation parameter [1–3]. For nuclei in this region, the $h_{11/2}$ orbital for both protons and neutrons lies close to the Fermi surface. For protons, the surface lies in the lower part of the shell, favoring a prolate deformed shape, and the neutron Fermi surface lies in the upper part of the $h_{11/2}$ shell, which favors oblate deformation [4]. The competing γ-driving effects of these high-j intruder orbitals can produce triaxial nuclear shapes in γ-soft nuclei. Additionally, the shape dependence of the underlying single-particle configuration of a nucleus can cause isomerism in γ-soft nuclei, where differing quasiparticle configurations may have differing nuclear shapes. Decays between states with different nuclear shapes are often strongly hindered as they require the rearrangement of a large number of nucleons.

Previous studies have established the presence of two isomeric states in ^{142}Tb: a 303 ms, $I^\pi = 5^-$ state [5] and a state higher in excitation energy with a tentative spin and parity assignment of $I^\pi = 8^+$ and a half-life in the microsecond range [6–8]. A detailed analysis of the delayed decay of these isomers was reported in Ref. [7] and the spin and

parity of the ^{142m2}Tb isomer was determined to be $I^\pi = 8^+$ through internal conversion analysis [7]. States built upon this $I^\pi = 8^+$ microsecond isomer were tentatively assigned using the Recoil-Isomer Tagging (RIT) method with the gas-filled recoil separator RITU [9,10] at the University of Jyväskylä, Finland [8]. The statistics in that experiment did not allow γ-γ coincidences to be examined beyond the three strongest transitions and the level scheme above the $I^\pi = 8^+$ isomer was based largely upon the observed γ-ray intensities [8].

In this article, we report the results of an experiment utilizing the JUROGAM target-position Ge-detector array and the GREAT focal-plane clover and planar detectors [11] coupled to the gas-filled recoil separator RITU [9,10]. This setup had a significantly increased recoil-isomer tagging efficiency compared with the previous RIT experiment [8] and allowed recoil-isomer tagged γ-γ coincidences for the transitions above the $I^\pi = 8^+$ isomer to be examined more extensively. The selectivity of the isomer-tagging technique for isolating weak channels in this region was also demonstrated in this experiment. Even when the prompt transitions above the isomer were known, it remained difficult to obtain clean spectra using triple γ-ray coincidences from the JUROGAM array alone.

This work has focused on the prompt states above the known ^{142m2}Tb isomeric $I^\pi = 8^+$ state with a view to examine the underlying single-particle configuration of the isomer. γ-ray transitions above and below the ^{142m2}Tb isomer were correlated and the level scheme above the isomeric state was extended. Angular distribution measurements were made for some of the more strongly populated transitions above the isomer, allowing the spins of these states to be inferred. Additionally, two

---

*Present address: Oliver Lodge Laboratory, University of Liverpool, Liverpool L69 7ZE, United Kingdom.

†Present address: STUK, Rovaniemi, Finland.

‡Present address: Instituut voor Kern-en Stralingsfysica, University of Leuven, Celestijnenlaan 200 D, B-3001 Leuven, Belgium.

previously unobserved prompt bands in ^{142}Tb were established that bypass the isomeric state. The configurations of the bands have been interpreted within the framework of the cranked-shell model and the properties of the aligned angular momentum, signature splitting, and $B(M1)/B(E2)$ values have been compared with the systematics in the neighboring nuclei. These comparisons give further evidence that the isomeric state was built upon a $\nu h_{11/2} \otimes \pi h_{11/2}$ configuration. The reduced transition probability for the $E1$ transition that depopulates the isomer was found to be consistent with those from similar isomeric states in the $N = 77$ isotones.

II. EXPERIMENT AND DATA ANALYSIS

To populate excited states in ^{142}Tb, a ^{54}Fe beam was accelerated onto a ^{92}Mo target of thickness $\sim$500 μg/cm^2 at energies of 245, 252, and 265 MeV using the K130 cyclotron at the University of Jyväskylä, Finland. The compound nucleus, ^{146}Er, promptly decayed via numerous exit channels to form neutron-deficient nuclei in the mass $A \sim 140$ region. The average beam current was $\sim$6.4 particle-nA (pnA) at 245 MeV, $\sim$8.2 pnA at 252 MeV, and $\sim$7.3 pnA at 265 MeV and the running times for each beam energy were approximately 30, 18, and 17 h, respectively. Prompt γ-ray decays were detected using the JUROGAM array, consisting of 43 Compton-suppressed HPGe detectors surrounding the target chamber of the gas-filled recoil separator RITU (Recoil Ion Transport Unit) [9]. Only 26 of the JUROGAM detectors were available for use during this experiment, reducing the photopeak efficiency from $4.2 \pm 0.1\%$ at 1332 MeV [12] to $\sim$2.5%. The recoiling fusion-evaporation residues were separated from any beam-like particles in RITU and were then transported into the GREAT focal-plane spectrometer [11], where γ-ray transitions delayed by an isomeric state were measured. Delayed γ-ray detection in the GREAT spectrometer was provided by a planar germanium detector with a high efficiency for x rays and low-energy γ rays and a clover germanium detector for the detection of higher-energy γ rays. The flight time of the recoils through RITU was approximately 0.5 μs; therefore only γ rays delayed by isomers with lifetimes greater than a few hundred nanoseconds were detected at the focal plane.

For this experiment, a nonstandard configuration of the GREAT focal-plane spectrometer was used in an attempt to increase the maximum beam intensity that could be used. In the standard GREAT configuration [11], the recoiling nuclei pass through a gas-filled multiwire proportional counter (MWPC) and are implanted into Double-sided Silicon Strip Detectors (DSSDs). The DSSDs produce a signal when a recoil is implanted, so that decays recorded in the JUROGAM and GREAT detectors can be associated with a successful recoil transmission through RITU. The DSSDs, in conjunction with the MWPC, also measure the time-of-flight (TOF) of the recoiling nuclei. The TOF measurement is used along with an energy-loss measurement from the MWPC to distinguish the desired reaction products from any unwanted scattered beam that is transmitted through RITU. Experiments utilizing the DSSDs are normally limited to recoil implantation rates of

$\sim$5 kHz to minimize radiation damage to the detectors. In this experiment the DSSDs were replaced with a second MWPC and recoils were implanted into a thin aluminium stopper foil placed after the second MWPC. The reason for the new setup was to allow the use of higher beam intensities to access nuclei with low production cross sections. However, in the revised setup it was found that the beam intensity was still limited to $\sim$7 pnA, corresponding to a recoil rate of $\sim$7.5 kHz in the second MWPC, as the maximum count rate for the JUROGAM detectors was also reached at this beam current. Although no significant increase to the beam intensity could be made, the dual-MWPC configuration proved to be 30% more efficient at this beam intensity for recoil isomer tagging experiments compared to the standard GREAT configuration.

Data collected during the experiment were acquired using the triggerless Total Data Readout (TDR) system [13], where each recorded decay was associated with a time stamp generated by a global 100-MHz clock. These data were sorted on- and offline using the GRAIN software package [14]. Data were sorted into a series of two- and three-dimensional spectra (matrices and cubes), which were analyzed using the UPAK [15] and RADWARE [16] software suites. In this report, γ rays detected at the target position are termed "prompt" and those detected at the focal plane are termed "delayed." The experiment used the recoil-isomer tagging technique [17], which correlates prompt and delayed γ rays across an isomeric state in prompt versus delayed matrices. Various time conditions can be applied to these matrices to optimize the sensitivity for isomeric decays with different half-lives.

III. RESULTS

Due to the time-correlation constraints of the experimental technique, the decay of the lower lying 303 ms ^{142m1}Tb [5] isomeric state was not observed in this study. The lifetime of the ^{142m2}Tb state has been measured previously as 15(4) μs [6] and 25(1) μs [7]. The recoil isomer tagging technique has also been previously used to establish the first evidence for prompt transitions above the ^{142m2}Tb isomeric state [8].

To examine the prompt transitions feeding the ^{142m2}Tb isomer in this experiment a prompt versus delayed matrix was constructed with the condition that the delayed decays must be detected within 60 μs of a recoil passing through the first GREAT MWPC. Summing energy gates set on the known 37-, 137-, 165-, and 303-keV [6–8] delayed transitions revealed the prompt transitions above the isomer, see Fig. 1(a). Gates were also set on the strongest of these prompt γ rays to project out the ^{142m2}Tb delayed γ rays and confirm the correlations. Angular distributions were measured for the most intense prompt transitions by determining their intensities in isomer tagged spectra for the individual detector rings of the JUROGAM array. These intensities were fitted with Legendre polynomials of the form $W(\theta) = A_0 + A_2 P_2(\cos\theta) + A_4 P_4(\cos\theta)$ as described by Yamazaki [18]. Table I lists the energies, intensities, and $A_{2,4}$ coefficients for ^{142}Tb γ rays observed in this study.

The statistics obtained in this study were sufficient to allow construction of a prompt γ-γ matrix correlated with the

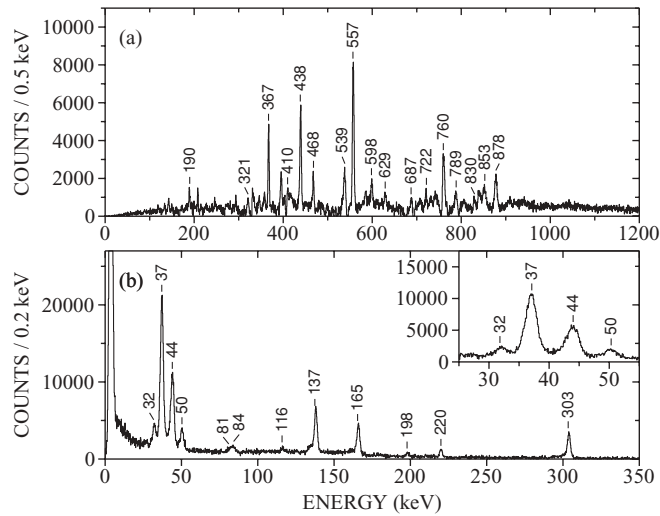FIG. 1. (a) The sum of γ-ray spectra created by gating on the delayed 37-, 137-, 165-, and 303-keV γ rays of ^{142}Tb in the prompt-delayed matrix, showing the prompt transitions above the ^{142m2}Tb isomeric state. (b) The sum of spectra created by gating on the 367-, 439-, 557-, 760-, and 878-keV prompt transitions in the prompt-delayed matrix, showing the γ rays below the ^{142m2}Tb isomeric state. The inset in panel (b) shows the low-energy delayed transitions expanded for clarity. All labeled peaks have been assigned to ^{142}Tb. The 44- and 50-keV peaks are the Tb K_{α} and K_{β} x rays respectively, aiding verification of the assignment of the observed transitions to ^{142}Tb. The scale for the inset to panel (b) shows counts/0.1 keV.

delayed transitions below the ^{142m2}Tb isomer. Only prompt γ-γ coincidences correlated with a 37-, 137-, 165-, or 303-keV delayed transition, detected in the GREAT Ge detectors within 60 μs of a recoil passing through the first GREAT MWPC, were incremented into the matrix. The matrix was also background subtracted in time and energy, providing a very clean matrix from which the prompt level scheme could be constructed. A prompt γ-γ matrix and prompt γ-γ-γ cube were also constructed, without the delayed correlations, allowing transitions bypassing the isomer to be observed, along with verification of the scheme above the isomer. The level scheme deduced from this study is shown in Fig. 2.

A. States below the ^{142m2}Tb isomer

The delayed transitions observed in this work largely confirm the delayed level scheme constructed in Ref. [7]. However, the tentatively proposed 335- and 340-keV transitions were not observed, see Fig. 1(b). Additionally, the 303-keV transition, previously assigned as having a mixed $M1/E2$ multipolarity [7], is assumed to be an $E2$ transition in this work and is placed as the lowest rotational transition in Band 3 as it provides a smooth extension of the band. Although the transition was previously assigned with a mixed $M1/E2$ mulitpolarity, the internal conversion coefficients measured for the 303-keV γ ray in Ref. [7] are consistent with a pure $E2$ transition. The determination of the multipolarity of this transition was not possible in this work, but the assumption that the 303-keV γ

TABLE I. γ-ray energies, intensities, initial and final spins, and angular coefficients for ^{142}Tb deduced in this work. The intensities are corrected for detector efficiency. Prompt and delayed transitions are normalized separately. *Value represents the combined intensity for the 81- and 84-keV doublet.

E_{γ} (keV)	I_{γ}	J_i^{π}	$\rightarrow$	J_f^{π}	A_2	A_4
			Delayed γ rays			
32.1(2)	9(2)	(5^-)	$\rightarrow$	5^-		
37.1(1)	100(3)	8^+	$\rightarrow$	7^-		
81(1)	10(2)*	6^-	$\rightarrow$	6^-		
84(1)	10(2)*	6^-	$\rightarrow$	(5^-)		
116.3(5)	4(1)	6^-	$\rightarrow$	5^-		
137.2(5)	37(9)	7^-	$\rightarrow$	6^-		
165.9(2)	32(2)	6^-	$\rightarrow$	(5^-)		
198.3(4)	6(2)	6^-	$\rightarrow$	5^-		
220.0(3)	13(3)	7^-	$\rightarrow$	6^-		
303.3(5)	67(13)	7^-	$\rightarrow$	(5^-)		
			Prompt γ rays			
133.6(2)	11(2)					
141.9(2)	19(2)					
189.2(5)	5(2)	10^+	$\rightarrow$	9^+		
232.7(3)	34(4)		$\rightarrow$	6^-		
321.1(2)	11(4)	12^+	$\rightarrow$	11^+		
367.3(1)	32(3)	8^+	$\rightarrow$	9^+	$-0.4(1)$	$-0.1(1)$
393.5(3)	19(5)					
402.2(3)	21(6)					
410.4(2)	10(4)	(14^+)	$\rightarrow$	(13^+)		
438.4(1)	61(2)	11^+	$\rightarrow$	10^+	$-0.18(6)$	$0.0(1)$
468.1(3)	26(2)	(13^+)	$\rightarrow$	12^+		
502.4(3)	55(8)	(9^-)	$\rightarrow$	7^-		
538.6(2)	44(3)		$\rightarrow$	9^+		
557.3(1)	100(6)	10^+	$\rightarrow$	8^+	$0.40(6)$	$0.0(1)$
586.2(3)	38(5)					
598.4(3)	18(3)		$\rightarrow$	11^+		
629.0(5)	8(2)	11^+	$\rightarrow$	9^+		
672.8(3)	38(10)					
687.2(3)	16(4)					
706.8(2)	28(6)					
722.0(4)	13(3)					
731.9(3)	15(6)					
746.6(3)	25(8)					
760.1(1)	56(2)	12^+	$\rightarrow$	10^+	$0.48(8)$	$0.0(1)$
772.4(3)	15(8)					
776.9(3)	19(8)					
788.5(3)	13(4)					
788.7(2)	26(4)	(13^+)	$\rightarrow$	11^+		
830.2(3)	13(5)	(18^+)	$\rightarrow$	(16^+)		
852.6(3)	39(6)	(16^+)	$\rightarrow$	(14^+)		
877.6(2)	44(4)	(14^+)	$\rightarrow$	12^+		
920.4(2)	6(2)					
1060.4(3)	6(2)					
1200.4(5)	2(1)					

ray is a rotational $E2$ transition changes the spins of the states below the ^{142m2}Tb isomer from those assigned in Ref. [7]. To retain consistency with the multipolarities adopted for the other firmly placed transitions from Ref. [7], the spin of the
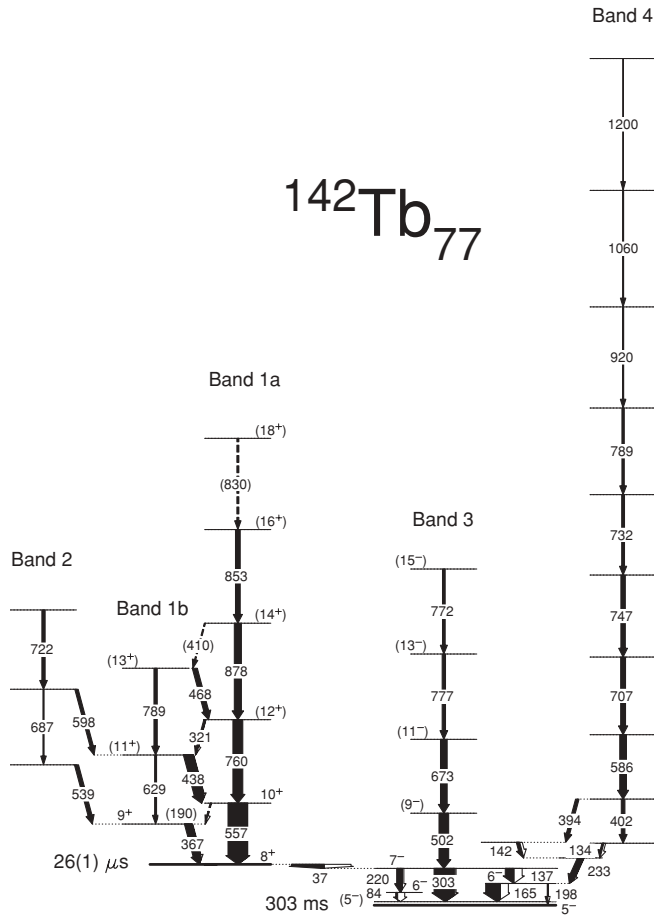
FIG. 2. The partial level scheme for ^{142}Tb deduced from this study. The widths of the arrows are proportional to the intensities of the γ-ray transitions and the white part of the arrows represents the calculated internal conversion component. Only the main decays below the ^{142m2}Tb state are shown. The nontentative spin assinments in this level scheme are based on the assignment of $I^{\pi} = 5^-$ for the ^{142m1}Tb isomer from Ref. [5] and an assignment of $I^{\pi} = 8^+$ for the ^{142m2}Tb isomer from Ref. [7] based on the systematics of neighboring nuclei and an internal conversion analysis of the transitions below the ^{142m2}Tb isomeric state.

final state of the 303-keV transition is tentatively changed from $I^{\pi} = 6^-$ to $I^{\pi} = 5^-$.

B. Bands 1a, 1b, and 2

The 557-, 760-, and 878-keV prompt transitions in Band 1a were previously measured to be in coincidence with one another in Ref. [8], which assumed they form a rotational sequence. In the present work, analysis of the isomer-gated prompt γ-γ matrix confirmed this coincidence and extended the band with the addition of an 853-keV γ ray and the tentative assignment of an 830-keV transition above it. The result of gating on the 557-keV transition of Band 1a in the isomer-gated prompt γ-γ matrix can be seen in Fig. 3(a). The tentative 208- and 143-keV linking transitions proposed from isomer-tagged singles data in Ref. [8] were not observed in coincidence with the 557-keV γ ray in the present work
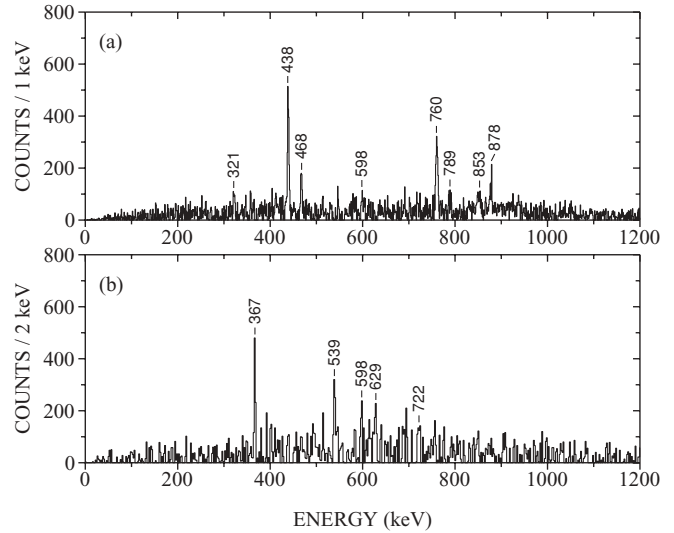

FIG. 3. (a) The spectrum of prompt γ rays in coincidence with the 557-keV γ ray in the recoil isomer tagged prompt γ-γ matrix, showing other γ rays in Bands 1a and 1b. (b) The sum of γ-ray spectra created by gating on the 367- and 539-keV γ rays in the same matrix showing transitions in Band 2.

and it was determined that the 557-keV transition feeds directly into the ^{142m2}Tb isomer. Band 1b, consisting of two transitions of 629 and 789 keV, appears to form a signature partner to Band 1a. A set of linking transitions between the Bands 1a and 1b was observed. The 190-keV linking transition is assigned as tentative because, although it appears in Fig. 1(a), it was difficult to confirm its coincidence with other prompt transitions directly, because of its low intensity. The energy of the 190-keV γ ray corresponds to the energy difference between the $I^{\pi} = 10^+$ and $I^{\pi} = 9^+$ levels, supporting its placement in the level scheme. The 687- and 722-keV transitions were assigned to Band 2, which links into Band 1 via transitions with energies of 539 and 598 keV. The transitions of Band 2 can be seen in Fig. 3(b), along with the linking transitions, created by summing spectra gated on the 367- and 539-keV transitions in the isomer-tagged prompt γ-γ matrix.

C. Bands 3 and 4

The 137-, 165-, 198-, 219-, and 303-keV γ rays below the ^{142m2}Tb state were also observed in the analysis of the prompt γ-γ-γ cube, indicating that there must be some additional prompt feeding of these states. By gating on these transitions in the cube, Bands 3 and 4, which bypass the ^{142m2}Tb isomer, were identified, see Fig. 2. Figure 4(a) shows a spectrum of γ rays in coincidence with the 672-keV γ ray projected from the prompt γ-γ matrix, showing the 137-, 165-, 219-, and 303-keV transitions. Figure 4(b) shows the sum of γ-ray spectra created by setting prompt γ-γ-γ coincidence gates on the 233-, 586-, 707-, 747-, 732-, 789-, 920-, 1060-, and 1200-keV transitions of band 4. The 324-keV γ ray in this spectrum could not be unambiguously placed in the level scheme. Angular distribution measurements could not be
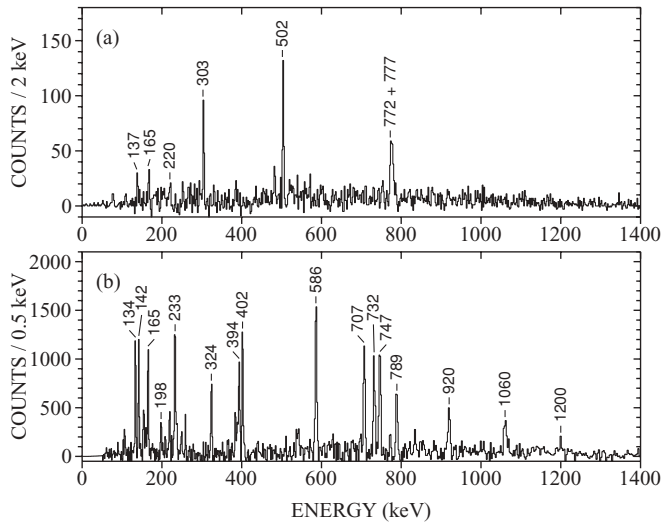
FIG. 4. (a) Spectrum of prompt γ rays in coincidence with the 673-keV γ ray in ^{142}Tb showing the other transitions in Band 3. The spectrum shows the 137-, 165-, 219-, and 303-keV γ rays, indicating that the band must bypass the ^{142m2}Tb isomeric state. (b) A sum of spectra created by setting γ-γ-γ coincidence gates on the 233-, 586-, 707-, 747-, 732-, 789-, 920-, 1060-, and 1200-keV transitions in Band 4, set in the prompt cube, showing the γ rays in Band 4.

obtained for the transitions in Band 4, but its bandhead spin was estimated to be between 6 and 10$\hbar$ as it feeds into an $I^{\pi} = 6^{-}$ state through two linking transitions of 134 and 233 keV.

D. Measurement of the ^{142m2}Tb half-life

The half-life of the ^{142m2}Tb was determined by making a series of focal-plane time spectra gated on the 137-, 165-, and 303-keV γ-ray transitions. The time parameter for these spectra is defined by the time difference between a recoil passing through the first MWPC and a γ ray being detected in the planar Ge detector, as measured by the global 100 MHz clock. A sample time spectrum for the 137-keV transition is shown in Fig. 5.

Half-lives were measured by fitting a sum of two exponentials to the spectra, with the second, longer-lived exponential representing the effect of random accidental correlations between recoils and γ rays. These accidental correlations arise where the detected γ ray is not associated with the last recoil detected at the focal plane. The decay constant for the shorter-lived exponential was corrected for random correlations as described in Ref. [19]. A weighted mean was taken of the individual results to give a half-life of 26(1) μs. The systematic error was estimated by taking the standard deviation of the half-lives found for each of the peaks at each beam energy. The systematic error associated with the background subtraction of the spectra was found to dominate over the statistical error in the fits, which was of the order of 0.1 μs. The result is consistent to within 3σ of the previous measurements of 15(4) μs [6] and 25(1) μs [7].
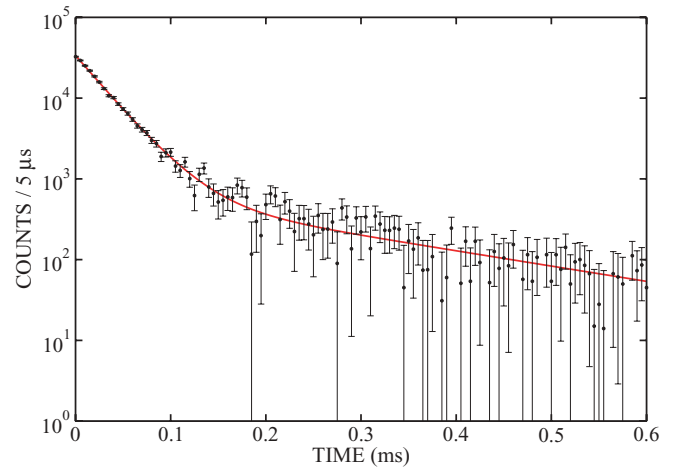

FIG. 5. (Color online) The time spectrum for the 137-keV peak collected with a beam energy of 245 MeV. The solid line represents the sum of twp fitted exponentials with half-lives of 21.8(2) and 159.3(4) μs. The errors in these two half-lives are solely from the statistical errors in the fitting process. The longer-lived component results from the effect of accidental correlations. The "TIME" axis label refers to the time difference between a recoil passing through the first MWPC and the γ ray being detected.

IV. DISCUSSION

The neutron-deficient mass 130–140 region of the nuclear chart is known to exhibit nuclear shapes that are triaxial or γ soft, a phenomenon that has been attributed to the shape driving effects of the competing $\pi h_{11/2}$ and $\nu h_{11/2}$ intruder orbitals [20,21]. The ^{142m2}Tb isomeric state is expected to have a configuration based on a $\pi h_{11/2} \otimes \nu h_{11/2}$ configuration, as the neighboring odd-proton nuclei (^{141,143}Tb) and odd-neutron nuclei (^{141}Gd, ^{143}Dy) have yrast bands built on $\pi h_{11/2}$ and $\nu h_{11/2}$ configurations, respectively [22–25]. Total Routhian surface (TRS) calculations were performed in Ref. [8] and predict a deformed nuclear shape with a large degree of triaxiality ($\beta_2 = 0.192$, $\beta_4 = -0.022$, and $\gamma = -30°$). Woods-Saxon cranked-shell model (CSM) calculations [26] were performed with these deformation parameters to aid the understanding of the underlying single-particle configurations for states observed in this work. The theoretical Routhians from these calculations are shown in Figs. 6 and 7 for quasiprotons and quasineutrons, respectively, taken from Ref. [8]. For a triaxial nucleus, Nilsson quantum numbers can no longer be used to describe the particle configurations and the only good quantum numbers are the parity, (π), and signature, (α). In this discussion, the configurations will be labeled by the standard convention for parity and signature. The negative-parity labels E and F refer to $(\pi, \alpha) = (-, -1/2)_1$ and $(-, +1/2)_1$, respectively, and the labels G and H refer to $(\pi, \alpha) = (-, -1/2)_2$ and $(-, +1/2)_2$, respectively. The positive-parity labels A and B refer to $(\pi, \alpha) = (+, +1/2)_1$ and $(+, -1/2)_1$, respectively. The negative-parity states are expected to largely be based on the $h_{11/2}$ orbital, though there will be smaller mixing contributions from the $f_{7/2}$ orbital, and the positive-parity states will contain contributions from the $g_{7/2}$, $d_{3/2}$, $d_{5/2}$, and $s_{1/2}$ orbitals [7,23,27].
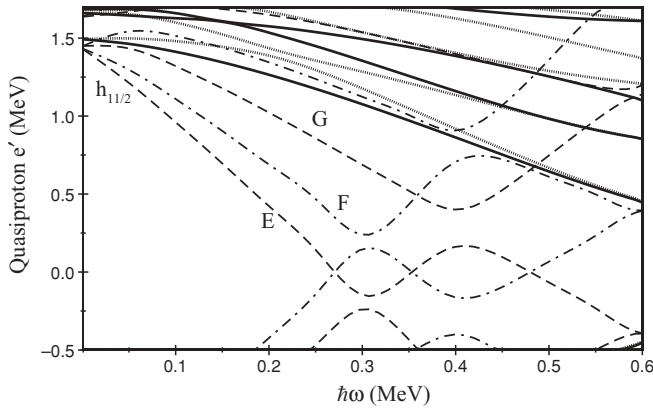
FIG. 6. Theoretical quasiproton Routhians, taken from Ref. [8], for ^{142}Tb from CSM calculations performed with deformation parameters $\beta_2 = 0.192$, $\beta_4 = -0.022$, and $\gamma = -30°$. The parity and signature, (π, α), of the Routhians are denoted by the line type. A solid line denotes $(\pi, \alpha) = (+, +1/2)$, a dotted line denotes $(\pi, \alpha) = (+, -1/2)$, a dash-dotted line refers to $(\pi, \alpha) = (-, +1/2)$, and a dashed line refers to $(\pi, \alpha) = (-, -1/2)$.

A. Bands 1a and 1b

Figure 8 shows the aligned angular momentum (alignment), i_x [28], versus rotational frequency for Bands 1a and 1b in this work along with the yrast bands from the neighboring nuclei $^{136}_{61}$Pm [29], $^{140}_{63}$Eu [27], and ^{143}Tb [23]. The yrast band of the odd-proton nucleus ^{143}Tb shows a gain in alignment of $\Delta I \approx 6\hbar$ at $\hbar\omega \approx 0.38$ MeV, which has been interpreted theoretically as the first-allowed proton crossing, π(FG), involving the second and third protons [23], see Fig. 6. No gain in alignment is observed for this band at $\hbar\omega \approx 0.3$ MeV, the expected frequency of the π(EF) crossing in Fig. 6. This indicates that this crossing must be blocked and so the yrast band of ^{143}Tb is assigned as being based on the first proton $\pi h_{11/2} E$ orbital [23]. A similar gain in alignment at $\hbar\omega \approx 0.38$ MeV is seen in the yrast bands of ^{141}Eu [30] and ^{139}Eu [31] and these bands are also interpreted as being based on the occupied πE orbital.
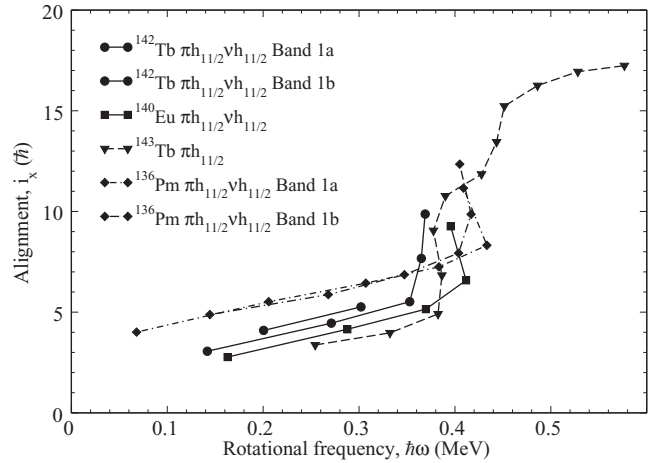

FIG. 8. The aligned angular momentum (alignment), i_x, versus rotational frequency for Bands 1a and 1b of ^{142}Tb from this work, along with the $\pi h_{11/2}$ yrast band of ^{143}Tb [23] and the $\pi h_{11/2} \otimes \nu h_{11/2}$ yrast bands of ^{140}Eu [27] and ^{136}Pm [29]. A reference band with Harris parameters [44] $\mathfrak{I}_0 = 12.0\hbar^2$ MeV^{-1} and $\mathfrak{I}_1 = 25.0\hbar^4$ MeV^{-3} [30] was subtracted from all the data in the figure and the bandhead spin of $I = 8$ was used as the K value for Bands 1a and 1b of ^{142}Tb.

Similarly, in this work Band 1a of ^{142}Tb does not show a gain in alignment at $\hbar\omega \approx 0.3$ MeV, suggesting that this band must also be built on a $\pi h_{11/2} E$ configuration coupled to an odd neutron. Band 1a does, however, show the beginnings of a backbend at $\hbar\omega \approx 0.37$ MeV, although the complete crossing is not observed. The similarities between this backbend and those observed at a similar frequency in ^{143}Tb, ^{141}Eu, and ^{139}Eu suggest that the π(FG) crossing is also responsible for the gain in alignment observed in Band 1a. The $\pi h_{11/2} \otimes \nu h_{11/2}$ yrast bands of ^{140}Eu [27] and ^{136}Pm [29,32], both built on $I^\pi = 8^+$ isomeric states, show alignment properties similar to those of Band 1a of ^{142}Tb, see Fig. 8. In both of these cases, the gain in alignment is also assigned as being due to the π(FG) crossing [27,29]. A $\pi E \nu F$ configuration is therefore also likely for the ^{142m2}Tb isomer as it is the lowest energy configuration that agrees with the observed alignment properties, signature, and $I^\pi = 8^+$ spin and parity assignment of this state.
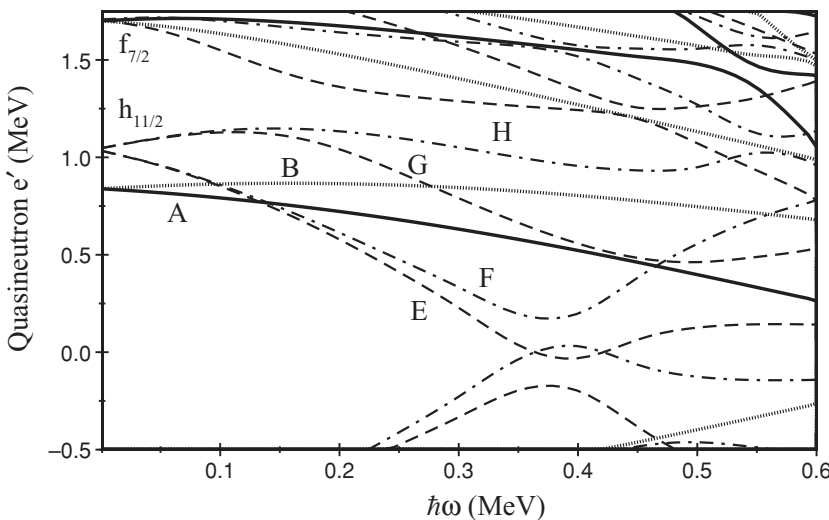

FIG. 7. Theoretical quasineutron Routhians, taken from Ref. [8], for ^{142}Tb from CSM calculations performed with deformation parameters $\beta_2 = 0.192$, $\beta_4 = -0.022$, and $\gamma = -30°$. The parity and signature, (π, α), of the Routhians are denoted by the line type. A solid line denotes $(\pi, \alpha) = (+, +1/2)$, a dotted line denotes $(\pi, \alpha) = (+, -1/2)$, a dash-dotted line refers to $(\pi, \alpha) = (-, +1/2)$, and a dashed line refers to $(\pi, \alpha) = (-, -1/2)$.

An alternative explanation for the backbend in Band 1a could instead be that the alignment is due to the first neutron ν(EF) crossing at $\hbar\omega \approx 0.4$ MeV, which occurs theoretically at a frequency similar to that of the π(FG) crossing, see Fig. 7. If the observed backbend was based on the ν(EF) crossing, then the ^{142m2}Tb isomeric state could not be built on the νE orbital as the crossing would be blocked. In this case, the odd neutron would be expected to reside in the higher-lying $\nu h_{11/2}H$ orbital rather than the positive-parity A and B orbitals, as these would give a negative parity for the state when coupled to a $\pi h_{11/2}$ orbital and hence not be in agreement with the assigned positive parity of the isomer. Without the observation of the full band crossing and determination of the total gain in alignment, it is difficult to unambiguously determine the configuration of the ^{142m2}Tb isomeric state from the two possibilities described. However, both cases support the expected $\pi h_{11/2} \otimes \nu h_{11/2}$ configuration as the most likely for this state. A $\pi E\nu F$ configuration is chosen as it lies lower in energy compared to a $\pi E\nu H$ configuration. As Band 1b appears to be the signature partner of Band 1a, it is assigned a $\pi h_{11/2} \otimes \nu h_{11/2}(\pi E\nu E)$ configuration, although the band is not extended to high enough spins to observe any backbending that might occur.

B. Bands 3 and 4

Figure 9 shows the aligned angular momentum versus rotational frequency for Bands 3 and 4 in this work along with the rotational band built on the $I^{\pi} = 5^{-}$ ^{140m1}Eu state [27], the yrast band of ^{141}Tb [22], and Band 1b of ^{143}Tb from Ref. [23]. A gain in alignment of $\Delta I \approx 8\hbar$ is seen for Band 4 at a rotational frequency of $\hbar\omega \approx 0.32$ MeV. Comparison with the theoretical quasiproton Routhians in Fig. 6 suggests that this is likely to be caused by the proton π(EF) crossing,
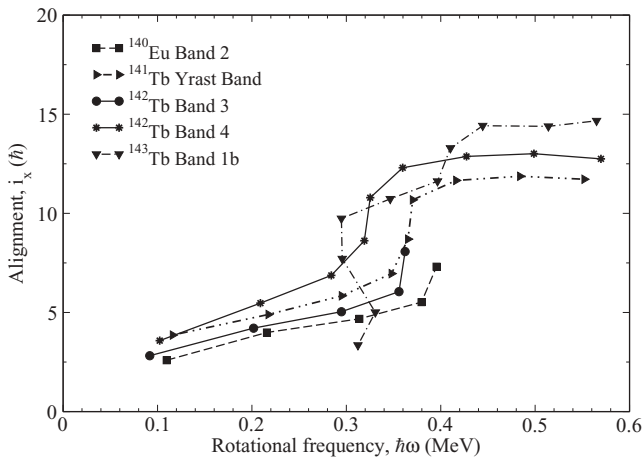

FIG. 9. The aligned angular momentum, i_x, versus rotational frequency for Bands 3 and 4 of ^{142}Tb from this work, along with Band 2 of ^{140}Eu from Ref. [27], the yrast band of ^{141}Tb [22], and Band 1b ^{143}Tb from Ref. [23]. A reference band with Harris parameters [44] $\Im_0 = 12.0\hbar^2$ MeV^{-1} and $\Im_1 = 25.0\hbar^4$MeV^{-3} [30] was subtracted from all the data in the figure. The bandhead spin of $I = (5)$ was used as the K value for Band 3 of ^{142}Tb and an estimated bandhead spin of $I = 8$ was used as the K value for Band 4.

indicating that the odd proton for this band cannot lie in the πE or πF $h_{11/2}$ orbitals. Band 1b of ^{143}Tb shows a similar gain in alignment at this frequency and this backbend was also interpreted as being due to the π(EF) crossing [23]. No gain in alignment is observed for Band 4 at $\hbar\omega \approx 0.4$ MeV, the expected frequency of the π(FG) crossing, so the odd proton for this band is likely to lie in the πG orbital, blocking the π(FG) crossing. The lack of a backbend at $\hbar\omega \approx 0.4$ MeV also indicates that the odd neutron for this band lies in the νE or νF orbitals, as the ν(EF) crossing is blocked. Band 4 is therefore assigned a $\pi h_{11/2} \otimes \nu h_{11/2} \pi G\nu E$ or $\pi G\nu F$ configuration. The spin and parity of the bandhead of Band 4 are not accurately known, but the $\pi h_{11/2} \otimes \nu h_{11/2}$ configuration is consistent with an estimated bandhead spin of between 6 and $10\hbar$.

As was stated previously, the 303-keV transition below the ^{142m2}Tb isomer is assigned to be the lowest energy transition of Band 3, feeding the bandhead of this band. Under this assumption, Band 3 shows a striking similarity to the yrast band of the neighboring odd-proton nucleus, ^{141}Tb [22], and to Band 2 of ^{140}Eu [27] in terms of level energy differences and alignment properties. The bands in ^{141}Tb and ^{140}Eu show a gain in alignment at $\hbar\omega \approx 0.38$ MeV, which is attributed to the π(FG) crossing. No gain in alignment is seen for Band 3 at $\hbar\omega \approx 0.3$ MeV, the expected frequency of the π(EF) crossing, indicating that it must be based on a $\pi h_{11/2}$ E coupled to an odd neutron. As with Band 1 of ^{142}Tb, a firm assignment for the neutron quasiparticle is difficult to make without extending Band 3 to higher spins. However, as the bandhead for Band 3 has a spin of $I^{\pi} = (5^{-})$, the lowest orbital consistent with the spin, parity, and signature of this state when coupled to a πE orbital is the νB orbital. Band 3 is therefore assigned a $\pi E\nu B$ configuration. The νB orbital is expected to contain contributions primarily from the $d_{3/2}$, $d_{5/2}$, and $s_{1/2}$ orbitals [7,23,27].

C. Signature splitting of bands 1a and 1b

Rotational bands built on triaxial nuclear shapes are expected to show signature splitting and particularly large signature splittings are expected for bands built upon high-j orbitals [1,33]. Signature splitting can be described in terms of a staggering parameter, $S(I)$ [34], defined as

$$S(I) = E(I) - E(I-1) - \tfrac{1}{2}[E(I+1) \\ - E(I) + E(I-1) - E(I-2)], \quad (1)$$

where $E(I)$ is the excitation energy of the level with spin I. Figure 10 shows the staggering parameters for Band 1 of ^{142}Tb from this work and the $\pi h_{11/2} \otimes \nu h_{11/2}$ band of the neighboring doubly odd $N = 77$ nucleus ^{140}Eu. Both bands show signature splitting consistent with a large deviation from axial symmetry [33].

Signature inversion is a common feature of bands built on $\pi h_{11/2} \otimes \nu h_{11/2}$ configurations in odd-odd nuclei in the neutron-deficient mass 120–140 region (e.g., ^{130,132}La, ^{134,136}Pm) [35]. This effect has been related to triaxial nuclear shapes with $\gamma < 30°$, along with a specific position of the Fermi surface within a given subshell [33]. It has also been
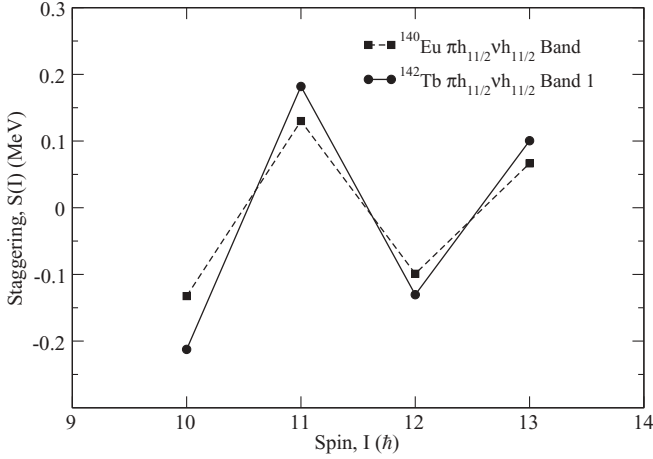
FIG. 10. The staggering parameter, $S(1)$, against spin for the $\pi h_{11/2} \otimes \nu h_{11/2}$ yrast bands of ^{140}Eu [27] and ^{142}Tb.
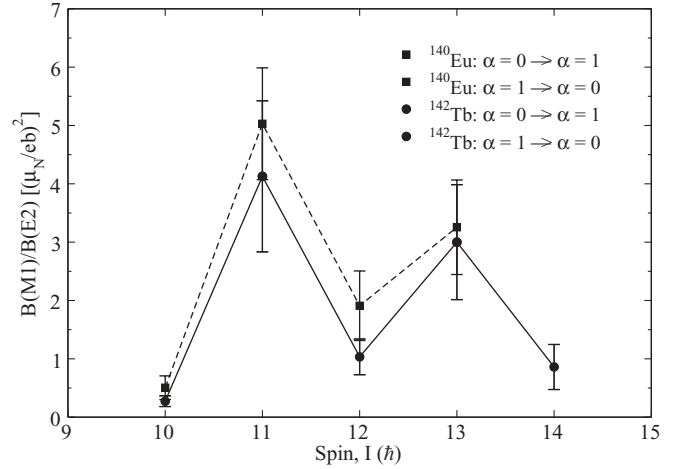

FIG. 11. The experimental $B(M1; I \rightarrow I - 1)/B(E2; I \rightarrow I - 2)$ ratios for Band 1 of ^{142}Tb and the $\pi h_{11/2} \otimes \nu h_{11/2}$ band of ^{140}Eu [27].

linked to a residual proton-neutron interaction, due to its observation only in two-quasiparticle configurations of odd-odd nuclei [36,37], and to the quadrupole-quadrupole pairing interaction [38].

The favored signature, α_f, for a two-quasiparticle band in an odd-odd nucleus is given by [39]

$$\alpha_f = \tfrac{1}{2}(-1)^{j_\pi - 1/2} + \tfrac{1}{2}(-1)^{j_\nu - 1/2}, \qquad (2)$$

where j_π and j_ν are the angular momenta of the proton and neutron quasiparticles, respectively. This gives $\alpha = 1$ as the favored signature for a $\pi h_{11/2} \otimes \nu h_{11/2}$ band. However, in Band 1, the theoretically unfavored $\alpha = 0$ signature is found to be lower in energy, which suggests that Band 1 is signature inverted. Further evidence for this signature inversion is provided by considering the differences in $B(M1; I \rightarrow I - 1)/B(E2; I \rightarrow I - 2)$ ratios, which are always larger for transitions from the favored to the unfavored signature, independent of any signature inversion effects. $B(M1; I \rightarrow I - 1)/B(E2; I \rightarrow I - 2)$ ratios were calculated from γ-ray branching ratios of $M1$ and $E2$ transitions from a state using

$$\frac{B(M1; I \rightarrow I - 1)}{B(E2; I \rightarrow I - 2)}$$
$$= 0.697 \frac{E_\gamma^5(I \rightarrow I - 2)}{E_\gamma^3(I \rightarrow I - 1)} \frac{I_\gamma(I \rightarrow I - 1)}{I_\gamma(I \rightarrow I - 2)}, \qquad (3)$$

where a mixing ratio of $\delta = 0$ was assumed. I_γ is the relative intensity of a transition and E_γ is its energy measured in MeV. The calculated $B(M1; I \rightarrow I - 1)/B(E2; I \rightarrow I - 2)$ ratios for Band 1 of ^{142}Tb and Band 1 of ^{140}Eu are shown in Fig. 11. For both nuclei, the $B(M1; I \rightarrow I - 1)/B(E2; I \rightarrow I - 2)$ ratios are seen to be larger for transitions from the higher energy signature partner (Band 1b of ^{142}Tb and Band 1a of ^{140}Eu from Ref. [27]), indicating that these bands are signature inverted. Also, the $B(M1; I \rightarrow I - 1)/B(E2; I \rightarrow I - 2)$ values in ^{142}Tb are very similar to those seen in ^{140}Eu, adding further weight to the $\pi h_{11/2} \otimes \nu h_{11/2}$ assignment for the ^{142m2}Tb isomeric state.

D. Lifetime of the isomeric state

The reduced transition probability for the 37-keV transition de-exciting the ^{142m2}Tb isomer is calculated to be $B(E1) = 1.1(1) \times 10^{-7}$ W.u using the Weisskopf single-particle estimate corrected for internal conversion. The neighboring doubly odd $N = 77$ isotones ^{140}Eu [27] and ^{144}Ho [8,40] also have $I^\pi = (8^+)$ isomers decaying via $E1$ transitions. The reduced transition probabilities for these decays are of a similar order of magnitude to that in ^{142}Tb despite differences in the lifetimes and energies of the transitions. The ^{140m2}Eu isomer decays through two $E1$ branches with energies of 37- and 98-keV and reduced transition probabilities of $7.6(6) \times 10^{-6}$ W.u and $1.4(1) \times 10^{-7}$ W.u, respectively [7,27]. The ^{144}Ho isomer, decaying through a 56-keV transition [8], has a reduced transition probability of $1.1(1) \times 10^{-6}$ W.u [8]. All of these reduced transition probabilities fall well within the recommended upper limits for $E1$ transitions in the $A = 91$–150 region [41]. A more detailed review of the transition probabilities for $E1$ decays in neutron-deficient $A \approx 140$ nuclei can be found in Ref. [32].

To understand the half-life of the ^{142m2}Tb isomeric state, several sources of hindrance for transitions from the isomer have been considered. As the isomer decays through an $E1$ γ-ray transition, the hindrance cannot be due to large changes in nuclear spin. Similarly, in this triaxial nucleus, K is not expected to be a good quantum number and therefore will not be conserved, implying no additional hindrance would be expected from a large reorientation of the nuclear spin with respect to the symmetry axis of the nucleus. However, a large change in the overlap of the two quasiparticles with the nuclear volume may contribute some hindrance in a similar manner to K hindrance.

The most likely cause of the hindrance for transitions from the ^{142m2}Tb isomer is through changes to the nuclear deformation. Shape isomers occur when several minima in the potential energy surface occur at different nuclear deformations and hence changes between these states are hindered. As was noted

earlier, $h_{11/2}$ proton orbitals are prolate driving while $h_{11/2}$ neutrons favor an oblate shape in neutron-deficient $A \sim 140$ nuclei. Because of these competing effects, a $\pi h_{11/2} \otimes \nu h_{11/2}$ two-quasiparticle configuration may be expected to have a triaxial shape. The 37-keV transition decays into Band 3, which is based on an $h_{11/2}$ proton coupled to a lower-j neutron quasiparticle. The lower-j quasiparticle will not show the shape driving effects of the $h_{11/2}$ neutron orbital and a quasiparticle configuration coupling this lower-j neutron to an $h_{11/2}$ proton may be expected to have a more prolate shape. For a transition between these two configurations, both a large change in the nuclear deformation and a reorientation in the nuclear spin with respect to the nuclear volume will be required. This will cause the transition to be hindered and cause the state to be isomeric. A series of detailed TRS calculations for each of these configurations in ^{142}Tb would be invaluable to help determine whether these differences in shapes are indeed responsible for the observed half-lives of these states.

V. CONCLUSIONS

In summary, use of the highly efficient JUROGAM target-position Ge-detector array coupled with the GREAT focal-plane spectrometer across the RITU gas-filled separator has significantly increased the efficiency of the isomer-tagging technique at the University of Jyväskylä. The rotational band built upon the $I^\pi = 8^+$ isomeric state in ^{142}Tb was established with isomer-tagged γ-γ coincidence data and angular distributions were measured for some of the more intensely populated states for the first time. The half-life of the isomer was remeasured to be 26(1) μs, which is

consistent, within 3σ, with previous results of 15(4) μs [6] and 25(1) μs [7]. Two promptly fed bands that bypassed the isomer were also established. These new data have been interpreted within the framework of the cranked-shell model and compared to the systematic behavior of the neighboring nuclei. These comparisons give evidence for a $\pi h_{11/2} \otimes \nu h_{11/2}$ configuration for the isomer and that its existence is likely due to shape differences between the isomer and the states to which it decays. Future measurements with this new efficient isomer-tagging setup are likely to reveal new information about these weakly populated structures in this neutron-deficient mass region near the proton drip line. Further advances to this technique [42,43] and new lifetime results for the states in the equivalent isomeric band in the neighboring $N = 77$ nucleus ^{144}Ho will soon be published by this Collaboration [40].

[1] Y. S. Chen, S. Frauendorf, and G. A. Leander, Phys. Rev. C **28**, 2437 (1983).

[2] I. Ragnarsson, A. Sobiczewski, R. K. Sheline, S. E. Larsson, and B. Nerlo-Pomorska, Nucl. Phys. **A233**, 329 (1974).

[3] C. W. Beausang, P. K. Weng, R. Ma, E. S. Paul, W. F. Piel, N. Xu, and D. B. Fossan, Phys. Rev. C **42**, 541 (1990).

[4] E. S. Paul et al., Phys. Rev. Lett. **58**, 984 (1987).

[5] R. B. Firestone, J. Gilat, J. M. Nitschke, P. A. Wilmarth, and K. S. Vierinen, Phys. Rev. C **43**, 1066 (1991).

[6] I. Zychor et al., GSI Annual Report 1988 GSI 89-1, 31 (1989).

[7] M. N. Tantawy et al., Phys. Rev. C **73**, 024316 (2006).

[8] C. Scholey et al., Phys. Rev. C **63**, 034321 (2001).

[9] M. Leino, J. Äystö, T. Enqvist, P. Heikkinen, A. Jokinen, M. Nurmia, A. Ostrowski, W. H. Trzaska, J. Uusitalo, K. Eskola, P. Armbruster, and V. Ninov, Nucl. Instrum. Methods Phys. Res. B **99**, 653 (1995).

[10] M. Leino, Nucl. Instrum. Methods Phys. Res. B **126**, 320 (1997).

[11] R. D. Page, A. N. Andreyev, D. E. Appelbe, P. A. Butler, S. J. Freeman, P. T. Greenlees, R. D. Herzberg, D. G. Jenkins, G. D. Jones, P. Jones, D. T. Joss, R. Julin, H. Kettunen, M. Leino, P. Rahkila, P. H. Regan, J. Simpson, J. Uusitalo, S. M. Vincent, and R. Wadsworth, Nucl. Instrum. Methods Phys. Res. B **204**, 634 (2003).

[12] P. T. Greenlees et al., Eur. Phys. J. A **25**, 599 (2005).

[13] I. Lazarus et al., IEEE Trans. Nucl. Sci. **48**, 567 (2001).

[14] P. Rahkila, Nucl. Instrum. Methods Phys. Res. A **595**, 637 (2008).

[15] W. T. Milner, UPAK, The Oak Ridge Analysis Package, Oak Ridge National Laboratory, Tennessee, 37831 (private communication).

[16] D. C. Radford, Nucl. Instrum. Methods Phys. Res. A **361**, 297 (1995).

[17] D. M. Cullen et al., Phys. Rev. C **58**, 846 (1998).

[18] T. Yamazaki, Nucl. Data A **3**, 1 (1967).

[19] M. E. Leino, S. Yashita, and A. Ghiorso, Phys. Rev. C **24**, 2370 (1981).

[20] R. Broda, Z. Phys. A **321**, 287 (1985).

[21] N. Redon, Z. Phys. A **325**, 127 (1986).

[22] N. H. Medina et al., Braz. J. Phys. **34**, 1002 (2004).

[23] F. R. Espinoza-Qui nones et al., Phys. Rev. C **60**, 054304 (1999).

[24] S. M. Mullins et al., Phys. Rev. C **47**, R2447 (1993).

[25] J. R. B. Oliveira et al., Phys. Rev. C **62**, 064301 (2000).

[26] W. Nazarewicz, R. Wyss, and A. Johnson, Nucl. Phys. **A503**, 285 (1989).

[27] D. M. Cullen et al., Phys. Rev. C **66**, 034308 (2002).

[28] R. Bengtsson and S. Frauendorf, Nucl. Phys. **A314**, 27 (1979).

[29] D. J. Hartley et al., Phys. Rev. C **64**, 031304(R) (2001).

[30] N. Xu et al., Phys. Rev. C **43**, 2189 (1991).

[31] P. Vaska *et al.*, Phys. Rev. C **52**, 1270 (1995).

[32] S. V. Rigby *et al.*, Phys. Rev. C **78**, 034304 (2008).

[33] R. Bengtsson *et al.*, Nucl. Phys. **A415**, 189 (1984).

[34] D. J. Hartley *et al.*, Phys. Rev. C **63**, 041301(R) (2001).

[35] Y. Liu, J. Lu, Y. Ma, S. Zhou, and H. Zheng, Phys. Rev. C **54**, 719 (1996).

[36] B. Cederwall *et al.*, Nucl. Phys. **A542**, 454 (1992).

[37] N. Tajima, Nucl. Phys. **A572**, 365 (1994).

[38] F. R. Xu, W. Satula, and R. Wyss, Nucl. Phys. **A669**, 119 (2000).

[39] I. Hamamoto, Phys. Lett. **B235**, 221 (1990).

[40] P. J. R. Mason *et al.* (unpublished).

[41] P. M. Endt, At. Data Nucl. Data Tables **26**, 41 (1981).

[42] D. M. Cullen *et al.*, AIP Conf. Proc. **1012**, 220 (2008).

[43] D. M. Cullen *et al.*, AIP Conf. Proc. **1072**, 185 (2009).

[44] S. M. Harris, Phys. Rev. **138**, B509 (1965).